Theoretical formulation of multiturn collective dynamics in a laser cavity modulator with comparison to Robinson and high-gain free-electron laser instability

Cheng-Ying Tsai*

School of Electrical and Electronic Engineering, Huazhong University of Science and Technology, Wuhan 430074, People's Republic of China

(Received 19 October 2021; accepted 23 May 2022; published 13 June 2022)

The study of collective beam instabilities has long been an important and active research topic in particle accelerators. The collective effects are typically divided into two categories: the short-range single-bunch instabilities and the long-range multibunch or multiturn instabilities. Robinson instability can be the mostly encountered long-range multiturn instability. We recently explored a collective multiturn instability driven by the short-range coherent undulator radiation in the laser cavity modulator of a steady-state microbunching (SSMB) storage ring. In this paper, we formulate and compare such an instability with the Robinson instability. Considering the radiation slippage effect and the finite duration, the functional form of the radiation wakes is essentially different from that of the Robinson case. We also relate a special case of the newly explored instability to the high-gain free-electron laser process and find that a similar cubic dispersion equation can be obtained. The discussions and comparisons presented in this paper may shed light on the underlying physical mechanisms of the collective beam dynamics in the laser cavity modulator of an SSMB storage ring.

DOI: 10.1103/PhysRevAccelBeams.25.064401

I. INTRODUCTION

The study of collective beam instabilities has long been an important and active research topic in particle accelerators, as the collective effects set important limitations on the beam intensity, the stability of machine operations, and the ultimate machine performances (see, for example, Refs. [1,2]). According to the length scales of wakefields, their effects may be typically divided into two categories: the short-range wakefield induced single-bunch instabilities and the long-range wakefield induced multibunch or multiturn instabilities. Typical examples of the former may include the single-bunch beam breakup (BBU) instability [3–5], the head-tail instability [6,7], the microbunching instability (MBI) in single-pass linear accelerators [8–13], in circular accelerators or storage rings [14–18], and in recirculating accelerators [19,20]. The latter category for the long-range instabilities is constituted by the subcases of the single-pass multibunch, multiturn single-bunch, or multiturn multibunch instabilities, e.g., the multibunch BBU [21–24], Robinson instability [25,26] (for more detailed introduction, see Refs. [1,2] and references therein). The concepts of the wakefield and impedance have long been developed and later become a building block of the standard collective instability analyses [1,2,27,28]. It should be mentioned that the analyses of the aforementioned collective effects usually neglect any possible slippage between the wakefields and the test particles during the beam-wake interaction. In addition to the above two categories, the free-electron laser (FEL) instability [29] may be classified as a separate, third one because the essence involves the radiation slippage in the beam-wake interaction.

As mentioned, the types of collective dynamics depend on the characteristic wavelength of the wake function or the characteristic frequency of the corresponding impedance spectrum. In a radio-frequency (rf) cavity, those frequencies largely satisfying the cavity resonance condition will be trapped inside the cavity structure and more or less form a discrete spectrum. The decay rate of the wakefield amplitude can be determined by the quality factor Q. In contrast, fields at frequencies higher than c/b, with b the beam pipe radius, will leak out of the cavity and propagate in the beam pipe, establishing a continuous spectrum. Since the typical bunch length in an electron storage ring lies in the millimeter (mm) range, the collective beam motions subject to the rf cavity induced wakefields belong to the long-ranged, multiturn dynamics. For a radiation field, e.g., the coherent synchrotron radiation (CSR) generated by an

*jcytsai@hust.edu.cn

electron traversing a bending magnet, it typically exhibits a broadband impedance [30–34]. Such a beam-wake interaction would result in a self-modulation in the beam phase space distribution, leading to the so-called microbunching or microwave instability [8–20]. The CSR may also occur in an undulator [35] and establishes both broadband and narrowband impedance spectrum. The resonant peaks with relatively high Q values locate around the undulator resonant frequency and its integer multiples [36]. The collective beam dynamics subject to the coherent radiation effects can be referred to as single-bunch or multibunch, depending on the bunch length, bunch spacing, and the characteristic length of the beam-wake interaction.

A typical rf cavity in a conventional storage ring plays two key roles: to boost or compensate for energy loss and to provide longitudinal focusing for a circulating electron bunch. A specialized cavity design, e.g., a harmonic rf cavity, may aim to manipulate the bunch in order to mitigate the coupled-bunch instabilities [37]. The recently proposed steady-state microbunching (SSMB) concept [38–43] may separate the aforementioned roles in two independent devices. An induction linac may be used to compensate for the energy loss due to synchrotron and undulator radiation emissions, while a laser modulator can be employed to provide the longitudinal focusing. An enhancement cavity may be installed to further increase the longitudinal focusing, called the laser cavity modulator. Due to the replacement of an rf cavity by the laser modulator in the SSMB storage ring, the distance between the adjacent bunches can be very small, in fact 5 orders of magnitude smaller, compared with that in a conventional rf-based storage ring. These closely spaced electron bunches form a microbunch train. In the situation when the undulator configuration remains the same, the radiation wake function generated by the traversing electron bunch can now introduce a relatively *long-range* beam-wake interaction, with the characteristic length compared with the bunch spacing and the microbunch length. Such a long-range radiation wake may bring about new instability mechanisms, e.g., the recently explored single-pass multibunch instability [44] or the single-bunch multiturn instability [45].

The above mentioned single-pass multibunch instability can be considered as a longitudinal BBU in the undulator of a laser modulator. A laser modulator, being a single-pass device, contains an external laser with an undulator, along which the laser and the electron resonate and copropagate. The external laser and the undulator magnetic field will form a phase space bucket to provide longitudinal focusing for an electron beam. Let us now consider the single-bunch multiturn instability [45] in the laser cavity modulator of an SSMB storage ring. A laser cavity modulator is now a multipass device and is comprised of an external laser, an undulator, and a set of cavity mirrors to store and accumulate the laser fields. When an electron bunch traverses the undulator, it emits coherent undulator radiation. After the electron bunch leaves the undulator, it would no longer emit radiation but the already generated radiation fields will be trapped inside the cavity. Due to the resonance condition, the undulator radiation wavelength is close to the central wavelength of the external laser and can be as well stored inside the cavity for a while. To ensure effective interaction of the external laser with the circulating electron bunch (in order to provide longitudinal focusing) requires their phase to be locked. Such a phase lock guarantees that the electron bunch would see the same phase space bucket when completing a revolution and returning back to the undulator entrance. Inside the undulator, the electron bunch will receive energy kicks of radiation wake functions period by period from the previous turns. As the radiation fields would have been stored in the cavity for a long time, a circulating electron beam perturbed by the radiation fields turn by turn may eventually become unstable. Possible differences between the radiation wake and the conventional one lie in the former being a finite duration and propagating inside the cavity. In contrast, the conventional wake is localized in a cavity structure and the decay rate of the field amplitude is determined by the cavity Q factor. Moreover, the summation of the generated wake functions is of convolution type for the case of the conventional rf cavity wake, while of nonconvolution type for the case of the coherent undulator radiations in the SSMB storage ring.

In this paper, we extend from the instability analyses [44,45] to more systematic discussions and comparisons of the aforementioned different situations. We will formulate the two problems, the Robinson instability and the recently explored multiturn instability in a laser cavity modulator, by writing the macroparticle equations of motion (as the difference equations) and solving for the asymptotic behaviors of the instabilities. We will begin from Robinson instability and obtain the existing results based on the z-transform. Following a similar treatment, we formulate the coherent radiation induced multiturn instability in an SSMB storage ring. Considering the radiation slippage effect and the finite duration, the functional form of the radiation wake is essentially different from the Robinson case. As a special case of the radiation wake, we relate the multiturn instability in an SSMB storage ring to the FEL instability, finding that a similar cubic dispersion or secular equation can be obtained.

It deserves here to summarize the contributions of this paper. First, we formulate a new instability mechanism, the coherent undulator radiation induced long-range single-bunch instability in the cavity modulator of an SSMB storage ring. Second, we compare the instability with the classic Robinson instability, particularly the essence that leads to the cubic and quadratic dispersion equations. Finally, we apply our developed formulation to a special case, which we relate to the FEL instability. It is hoped that the discussions and comparisons presented in this paper

may shed light on the underlying physical mechanisms of collective beam dynamics in the laser cavity modulator.

This paper is organized as follows: In Sec. II, we review the theoretical formulation of Robinson instability based on the macroparticle model, solve for the dispersion or secular equation, and illustrate a simple practical example. As a recently explored collective effect, the coherent undulator radiation induced single-bunch multiturn instability is then introduced and analyzed in Sec. III with a set of preliminary SSMB laser modulator design parameters as an example. Section IV discusses and compares the Robinson instability and the recently explored multiturn instability in the laser cavity modulator, particularly the differences between the wake function and the resultant dispersion equation. As a special case, we relate the multiturn instability to the FEL instability and obtain a similar cubic dispersion equation, elaborated in Sec. V. Finally, we summarize the main results in Sec. VI.

II. ROBINSON INSTABILITY DRIVEN BY RF CAVITY WAKEFIELD

In this section, we outline a typical single-bunch multiturn instability mostly encountered in circular accelerators, called Robinson instability [1,2,25,26]. There have been developed many different approaches to analyze such an instability; here the macroparticle model will be adopted. By defining the relative energy deviation of the macroparticle as $\delta = \frac{\gamma\gamma_0}{\gamma_0}$ with γ_0 the Lorentz relativistic factor of the on-momentum reference energy, the physical mechanism can be described as follows. Consider a storage ring operating above transition with phase stability, if an electron with $\delta > 0$ will lose less energy than that of an electron with $\delta < 0$ due to the rf cavity induced wakefield turn after turn, one expects that the beam will soon become unstable. This undesired situation indeed occurs when the frequency of the rf cavity ω_R is lower than the harmonics of the revolution frequency $h\omega_0$ with h the harmonic number. In the following subsection, we will reformulate the Robinson instability.

A. Theoretical formulation

First, the rf cavity impedance can be well described by an *RLC*-type impedance. For the single-mode case, the longitudinal impedance can be written as [1,2]

$$Z_{\parallel}(\omega) = \frac{R_S}{1 + iQ(\frac{\omega_R}{\omega} - \frac{\omega}{\omega_R})}, \tag{1}$$

where ω_R is the natural resonant frequency of the rf cavity, R_S is the shunt impedance, and Q is the quality factor. Here, a fine-tuning of ω_R can be allowed. The corresponding wake function can be derived by the following definition:

$$W_{\parallel}(z) = \frac{1}{2\pi}\int_{-\infty}^{\infty} Z_{\parallel}(\omega) e^{i\frac{\omega}{c}z} \mathrm{d}\omega, \tag{2}$$

where $z < 0$ refers to the tail of the source particle and c is the speed of light. There is no rf cavity wake ahead of the source particle, i.e., $W_{\parallel}(z > 0) = 0$. Substituting Eq. (1) into Eq. (2), the wake function can be analytically obtained [1,2]

$$W_{\parallel}(z < 0) = 2\alpha R_S e^{\alpha z/c}\left(\cos\frac{\bar{\omega}z}{c} + \frac{\alpha}{\bar{\omega}}\sin\frac{\bar{\omega}z}{c}\right), \tag{3}$$

where the damping coefficient $\alpha = \omega_R/2Q$ and $\bar{\omega} = \sqrt{\omega_R^2 - \alpha^2}$. When an electron traverses an rf cavity, it leaves a wake function as Eq. (3). The wake function starts to decay in time, while the electron circulates in the storage ring. When the electron comes back to the rf cavity, it would see the temporally decaying wake function. A moment's reflection will show that the electron bunch on the nth turn will experience the wake function from the kth turn $W_{\parallel}(kC - nC + z_n - z_k)$, with C being the storage ring circumference and z_n, z_k being the longitudinal displacement on the nth and kth turn, respectively. Due to $|(k-n)C| \gg |z_n - z_k|$, we may Taylor expand the wake function

$$W_{\parallel}(kC - nC + z_n - z_k) \approx W_{\parallel}(kC - nC) + W'_{\parallel}(kC - nC)(z_n - z_k), \tag{4}$$

where the first term on the right-hand side refers to the static parasitic loss, the second term $z_n W'_{\parallel}(kC - nC)$ characterizes the potential well distortion, and the third term $z_k W'_{\parallel}(kC - nC)$ serves as a resonant driving mechanism. It is the third term that leads to the Robinson instability.

Having obtained the proper argument of the wake function, we can formulate the macroparticle equations of motion. Since the entire bunch is represented as a macroparticle, only the bunch centroid or the dipole motion is revealed. The effects of the finite energy spread or the internal phase space structure would be excluded. Inside the rf cavity, we have

$$\begin{cases} z_{n,\mathrm{fin}} = z_{n,\mathrm{ini}} \\ \delta_{n,\mathrm{fin}} = \delta_{n,\mathrm{ini}} + \left[\frac{k_{s0}^2 C}{\eta} - \frac{4\pi\epsilon_0 N r_e}{\gamma_0}\sum_{k=0}^{n} W'_{\parallel}(kC - nC)\right] z_{n,\mathrm{ini}} + \frac{4\pi\epsilon_0 N r_e}{\gamma_0}\sum_{k=0}^{n} W'_{\parallel}(kC - nC) z_{k,\mathrm{ini}} \end{cases}, \tag{5}$$

where N is the number of electrons in the bunch, ϵ_0 is the vacuum permittivity, and r_e is the classical electron radius. The subscript n is used to denote the quantities on the nth turn, the subscript ini refers to the location at the rf cavity entrance, and fin to the rf cavity exit. The k_{s0} reflects the longitudinal focusing provided by the rf cavity. Outside the cavity in the remaining storage ring, we have

$$\begin{cases} z_{n+1,\mathrm{ini}} = z_{n,\mathrm{fin}} - \eta C \delta_{n,\mathrm{fin}} \\ \delta_{n+1,\mathrm{ini}} = \delta_{n,\mathrm{fin}} \end{cases}, \tag{6}$$

in which η is the storage ring phase slip factor. By writing down $\frac{k_{s0}^2 C}{\eta} z_n$ in Eq. (5), we have assumed that the bunch length is much shorter than the rf wavelength and the incoherent synchrotron radiation loss is compensated by the rf cavity. The original form may be written as $\frac{k_{s0}^2 C}{\eta k_R}(\sin k_R z_n - \sin\phi_s)$, with ϕ_s the synchronous phase and $k_R = \omega_R/c$. For the convenience of the following discussion, let us define a shorthand notation $\mathcal{W}'_{\parallel}(kC - nC) \equiv \frac{4\pi\epsilon_0 N r_e}{\gamma_0} W'_{\parallel}(kC - nC)$. The above Eqs. (5) and (6) may be cast into a matrix formalism

$$\begin{aligned} \begin{bmatrix} z \\ \delta \end{bmatrix}_{n+1,\mathrm{ini}} &= \begin{pmatrix} 1 & -\eta C \\ 0 & 1 \end{pmatrix} \begin{bmatrix} z \\ \delta \end{bmatrix}_{n,\mathrm{fin}} \\ &= \begin{pmatrix} 1 & -\eta C \\ 0 & 1 \end{pmatrix} \left\{ \begin{pmatrix} 1 & 0 \\ \frac{k_{s0}^2 C}{\eta} - \sum_{k=0}^{n} \mathcal{W}'_{\parallel}(kC - nC) & 1 \end{pmatrix} \begin{bmatrix} z \\ \delta \end{bmatrix}_{n,\mathrm{ini}} + \sum_{k=0}^{n} \begin{pmatrix} 0 & 0 \\ \mathcal{W}'_{\parallel}(kC - nC) & 0 \end{pmatrix} \begin{bmatrix} z \\ \delta \end{bmatrix}_{k,\mathrm{ini}} \right\} \end{aligned} \tag{7}$$

or in a compact form

$$Y_{n+1} = \mathbf{R}\left(\mathbf{M}_n Y_n + \sum_{k=0}^{n} \mathbf{W}_{n-k} Y_k \right), \tag{8}$$

with $Y = [z\delta]^T$. Neglecting the effect of the potential well distortion, i.e., dropping the time dependence of $\mathbf{M}$, we have

$$\begin{aligned} Y_{n+1} &\approx \begin{pmatrix} 1 - k_{s0}^2 C^2 & -\eta C \\ \frac{k_{s0}^2 C}{\eta} & 1 \end{pmatrix} Y_n + \sum_{k=0}^{n} \begin{pmatrix} 0 & 0 \\ \mathcal{W}'_{\parallel}(kC - nC) & 0 \end{pmatrix} Y_k \\ &= \mathbf{A} Y_n + \sum_{k=0}^{n} \mathbf{B}_{n-k} Y_k. \end{aligned} \tag{9}$$

Here we note that the 1×1 term of matrix $\mathbf{B}_{n-k}$ in Eq. (9) should be 0. The reason is that in the turn-by-turn analysis, the wake effect is considered a first-order effect in one revolution. The zeroth-order effect refers to the case of pure-optics transport. In the first-order analysis, the first-order wake effect shall correspond to the change of the particle's energy coordinate δ. In the same order, the change of the particle's position coordinate z due to δ should be accounted for. If the nonzero 1×1 element were retained, it means that within a single revolution the change of the particle's position coordinate z is not only from the first-order δ but also from the second-order correction of δ explicitly due to the wake. Since the analysis is assumed a first-order analysis, we neglect this second-order contribution.

Equation (9) is a standard matrix equation, representing a dynamical system with memory. The stability of Eq. (9) can be solved by the z-transform [46]. The z-transform of Y_n can be defined as

$$\mathcal{Z}[Y_n] = \tilde{Y}(\mathsf{z}) \equiv \sum_{j=0}^{\infty} Y_j \mathsf{z}^{-j} = Y_0 + Y_1 \mathsf{z}^{-1} + Y_2 \mathsf{z}^{-2} + \cdots. \tag{10}$$

Now let us take the z-transform on both sides of Eq. (9)

$$\mathsf{z}\tilde{Y}(\mathsf{z}) - \mathsf{z} Y_0 = \mathbf{A}\tilde{Y}(\mathsf{z}) + \tilde{\mathbf{B}}(\mathsf{z})\tilde{Y}(\mathsf{z}), \tag{11}$$

where we have used the convolution theorem

$$\mathcal{Z}\left[\sum_{k=0}^{n} \mathbf{B}_{n-k} Y_k \right] = \tilde{\mathbf{B}}(\mathsf{z})\tilde{Y}(\mathsf{z}) \tag{12}$$

and the shifting property

$$\mathcal{Z}[Y_{m+k}] = \mathsf{z}^k \tilde{Y}(\mathsf{z}) - \sum_{r=0}^{k-1} Y_r \mathsf{z}^{k-r}. \tag{13}$$

Solving Eq. (11) for $\tilde{Y}(\mathsf{z})$ gives

$$\tilde{Y}(\mathsf{z}) = \frac{\mathsf{z}}{\mathsf{z}\mathbb{I} - \mathbf{A} - \tilde{\mathbf{B}}(\mathsf{z})} Y_0, \tag{14}$$

with $\mathbb{I}$ the identity matrix.

The system stability is determined by $\det(\mathsf{z}\mathbb{I} - \mathbf{A} - \tilde{\mathbf{B}}(\mathsf{z})) = 0$ or

$$\det \begin{pmatrix} \mathsf{z} - 1 + k_{s0}^2 C^2 & \eta C \\ -\frac{k_{s0}^2 C}{\eta} - \tilde{\mathcal{W}}'_{\parallel}(\mathsf{z}) & \mathsf{z} - 1 \end{pmatrix} = 0, \tag{15}$$

where the explicit expression of $\tilde{\mathcal{W}}'_{\parallel}$ can be found in Appendix A [Eq. (A3)]. Note that $\tilde{\mathcal{W}}'_{\parallel}$ is not exactly equal to the impedance function $Z_{\parallel}$. Equation (15) can be expanded as

$$(\mathsf{z}-1)^2+\eta C\left[\frac{k_{s0}^2 C}{\eta}+\tilde{\mathcal{W}}_{\parallel}'(\mathsf{z})\right]=0. \tag{16}$$

For the moment we have obtained the dispersion or secular equation of the dynamical system. In the next subsection, we will solve Eq. (16) for the system (in)stability.

B. Solving secular equation

To solve the secular equation, Eq. (16), we let $\mathsf{z}=e^{i\Omega T_0}$ with T_0 the revolution period and Ω in general a complex quantity and assume $|\Omega T_0|\ll 1$. Substituting into Eq. (16) gives

$$-\Omega^2 T_0^2+k_{s0}^2 C+\eta C\tilde{\mathcal{W}}_{\parallel}'(\mathsf{z})=0. \tag{17}$$

After replacing $\tilde{\mathcal{W}}_{\parallel}'$ with the explicit expression Eq. (A3), Eq. (17) can be written in a familiar form

$$-\Omega^2 T_0^2+k_{s0}^2 C+i\frac{4\pi\epsilon_0 N r_e\eta}{\gamma_0}\times\sum_{p=-\infty}^{\infty}(\Omega+p\omega_0)Z_{\parallel}(\Omega+p\omega_0)=0 \tag{18}$$

or

$$\Omega^2-\omega_{s0}^2=i\frac{4\pi\epsilon_0 N r_e\eta}{\gamma_0 T_0^2}\sum_{p=-\infty}^{\infty}(\Omega+p\omega_0)Z_{\parallel}(\Omega+p\omega_0) \tag{19}$$

with $c=C/T_0$. Considering $\mathrm{Re}\Omega\approx\omega_{s0}$, we have the imaginary part that represents the instability growth rate

$$\tau^{-1}\equiv\mathrm{Im}(\Omega-\omega_{s0})\approx\frac{4\pi\epsilon_0 N r_e\eta}{2\gamma_0 T_0^2\omega_s^0}\times\sum_{p=-\infty}^{\infty}(\Omega+p\omega_0)\mathrm{Re}Z_{\parallel}(\Omega+p\omega_0), \tag{20}$$

where a negative value indicates that the system is unstable. There is a sign difference in Refs. [1,2] because of the different notations adopted. Equation (20) is a well-known result [1,2]. For the *RLC*-type narrowband impedance, $\omega_R\approx h\omega_0$, we have the simplified expression

$$\tau_{\mathrm{ana,Z}}^{-1}=\frac{2\pi\epsilon_0 N r_e\eta h\omega_0}{\gamma_0 T_0^2\omega_s}[\mathrm{Re}Z_{\parallel}(h\omega_0+\omega_s)-\mathrm{Re}Z_{\parallel}(h\omega_0-\omega_s)], \tag{21}$$

or, with substitution of Eq. (1) and assuming $\Delta\omega=\omega_R h\omega_0\ll\omega_R/2Q$ [1,2]

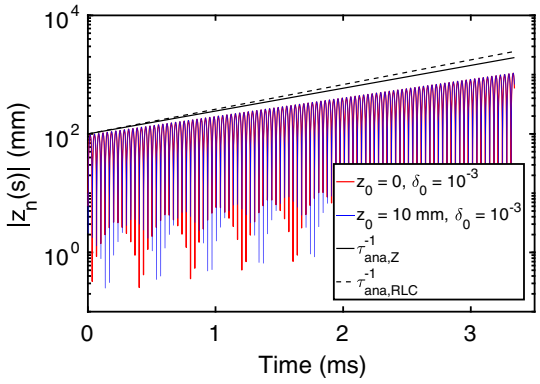

FIG. 1. Longitudinal displacement as a function of time. The red and blue lines are obtained by tracking simulations. The black solid and dashed lines are from analytical predictions, i.e., Eqs. (21) and (22), respectively.

$$\tau_{\mathrm{ana},RLC}^{-1}\approx\frac{4N r_e\eta R_S Q^2\Delta\omega}{\pi\gamma_0 T_0 h}. \tag{22}$$

Here we use $\tau_{\mathrm{ana,Z}}^{-1}$ to denote Eq. (21) because the respective impedances would be evaluated from Eq. (1). The $\tau_{\mathrm{ana},RLC}^{-1}$ stands for Eq. (22) based on the narrowband approximation. Before ending this subsection, we remind that at the beginning of this section, the described physical picture of Robinson instability can be confirmed by Eq. (21).

C. Example

In this subsection, we take a simple numerical example to illustrate the Robinson instability. Consider the beam and the storage ring parameters with $\eta=0.03$, $N=10^{11}$, the reference energy $E=1$ GeV, $\omega_0=9.4\times10^6$ rad/sec, $\nu_{s0}=0.01$, $h=240$, $h\omega_0/2\pi=360$ MHz, $R_S=1$ MΩ, $Q=2000$, and $\Delta\omega/2\pi=10$ kHz. According to Eq. (22) the predicted instability growth rate $\tau^{-1}\approx1.2$ ms. Given these input parameters, Fig. 1 shows the turn-by-turn tracking simulation results based on Eqs. (5) and (6). The theoretical predictions based on Eqs. (21) and (22) are also drawn in the figure, showing good agreement with tracking simulations. Besides, we see that different initial conditions only lead to a phase offset; the collective dynamical behaviors remain the same. The frequency detuning $\Delta\omega/2\pi>0$ is such that the beam becomes unstable for $\eta>0$; a proper detuning $\Delta\omega/2\pi<0$ would stabilize the beam.

III. MULTITURN INSTABILITY DRIVEN BY COHERENT RADIATION

In this section, we consider a recently explored instability mechanism, motivated by the recent proposal of the SSMB scheme in a storage ring [38]. A laser cavity modulator consists of an external laser, a set of cavity

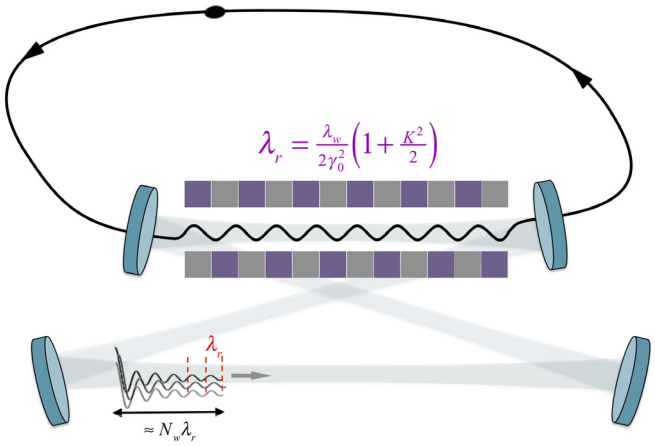

FIG. 2. Schematic layout of the SSMB storage ring with a laser cavity modulator. The laser fields, together with the undulator magnetic field, in the cavity provide longitudinal focusing to the circulating electron bunch. A N_w-period undulator will produce radiation wakefields, each with the finite duration $N_w\lambda_r$ with λ_r the undulator resonant wavelength. The propagating radiation fields bounce back and forth among the mirrors in the cavity modulator.

mirrors to accumulate a sufficient laser intensity, and an undulator. The external laser and the undulator magnetic field will form a series of phase space buckets, similar to the role of an rf cavity in a conventional storage ring. When the bunch traverses the undulator, it emits radiation. After the electron leaves the undulator, the generated radiation fields are confined in the laser cavity, for example, in the four-mirror ring cavity shown in Fig. 2. The phase-lock condition ensures that the electron bunch would meet the same phase space bucket when returning to the undulator entrance.

The finite duration of the radiation wake is $N_w\lambda_r$, with N_w the number of undulator periods and λ_r the undulator resonant wavelength. Different from the long-range wake induced in an rf cavity, the radiation wake in an undulator is relatively short-ranged. However, the radiation wakes propagate, bounce back and forth among the cavity mirrors, and meet/overlap the electron bunch completing one revolution in the remaining storage ring. Moreover, an electron traverses along the undulator at a certain passage at the speed of $\beta_z c$, while both the emitted radiation and the external laser propagate at the speed of light c. The speed difference results in the fact that the radiation fields slip over one resonant wavelength with respect to the electron per undulator period. The resulting beam dynamics may exhibit a long-range, multiturn behavior.

A. Theoretical formulation

The radiation wake function $W_\parallel$, emitted by an electron moving in an undulator, can be obtained by inverse Fourier transformation of the radiation impedance [1,2]

$$W_\parallel(z>0) = \frac{2c}{\pi}\int_0^\infty \mathrm{Re}Z_\parallel(k)\cos kz\mathrm{d}k, \tag{23}$$

where k is the wavenumber and Re takes the real part of the radiation impedance $Z_\parallel$. Here $z>0$ refers to the head of the source particle. In this expression, we require $W_\parallel(z<0)=0$. The undulator radiation impedance per unit length per unit undulator wavenumber at a specific harmonic can be written as [47–49]

$$\frac{\mathrm{Re}Z_\parallel(\omega)}{L_w k_w} = Z_0\bar{G}(\theta_1)\left(1+\frac{K^2}{2}\right)\left(\frac{\omega}{\omega_r}\right)^{-1}, \tag{24}$$

where $Z_0 \approx 377\ \Omega$ is the free space impedance, $k_w = 2\pi/\lambda_w$ with λ_w the undulator period, $L_w = N_w\lambda_w$ the undulator length with N_w the number of undulator periods. The frequency-dependent polar angle is $\theta_1 = \frac{1}{\gamma_0}\sqrt{(1+\frac{K^2}{2})(H\frac{\omega_r}{\omega}-1)}$, where the positive integer H is the harmonic number, K is dimensionless undulator parameter, and the resonant frequency $\omega_r = ck_r = 2\pi c/\lambda_r$ with the undulator resonant wavelength λ_r satisfying $\lambda_r = \frac{\lambda_w}{2\gamma_0^2}(1+\frac{K^2}{2})$. The azimuthal angle ϕ-averaged function

$$\bar{G}(\theta) = \frac{1}{2\pi}\int_0^{2\pi} G(\theta,\phi)\mathrm{d}\phi, \tag{25}$$

with $G(\theta,\phi) = G_\sigma(\theta,\phi) + G_\pi(\theta,\phi)$

$$G_\sigma(\theta,\phi) = \frac{1}{2}\left[\frac{H(K\mathcal{D}_1 + \gamma\theta\mathcal{D}_2\cos\phi)}{1+\frac{K^2}{2}+\gamma^2\theta^2}\right]^2 \tag{26}$$

and

$$G_\pi(\theta,\phi) = \frac{1}{2}\left(\frac{H\gamma\theta\mathcal{D}_2\sin\phi}{1+\frac{K^2}{2}+\gamma^2\theta^2}\right)^2, \tag{27}$$

where

$$\mathcal{D}_1 = -\frac{1}{2}\sum_{m=-\infty}^{\infty} J_{H+2m-1}(H\alpha)[J_m(H\zeta)+J_{m-1}(H\zeta)] \tag{28}$$

and

$$\mathcal{D}_2 = \sum_{m=-\infty}^{\infty} J_{H+2m}(H\alpha)J_m(H\zeta), \tag{29}$$

where J_m is the mth order Bessel function of the first kind, $\alpha = \frac{2K\gamma\theta\cos\phi}{1+\frac{K^2}{2}+\gamma^2\theta^2}$, $\zeta = \frac{K^2/4}{1+\frac{K^2}{2}+\gamma^2\theta^2}$.

When multiple harmonics are concerned, the overall radiation impedance function $\mathrm{Re}Z_\parallel$ can be obtained by summing the individual harmonic H in Eq. (24), i.e., $\mathrm{Re}Z_\parallel(\omega) = \sum_H \mathrm{Re}Z_{\parallel,H}(\omega)$. The corresponding radiation

wake function can be calculated via Eq. (23). For simplicity we consider only the fundamental harmonic $H = 1$ and assume the cavity mirrors are perfect. As for the choice of the maximum harmonic number and the possible effects of the cavity mirrors, the interested readers are referred to Refs. [44,45,50]. The proper argument of the radiation wake function can be inferred by the beam-wake interaction in the laser cavity modulator and the remaining storage ring, as we have outlined in the Introduction and the beginning of this section. A moments reflection reveals that a circulating electron at the nth undulator period on the mth turn will suffer the radiation wake of the following form:

$$\sum_{k=0}^{m-1}\sum_{p=0}^{n-1}\mathcal{W}_{\parallel}[(N_w-p)\lambda_r+z_m^{(p)}-z_k^{(0)}]. \tag{30}$$

Notice that the phase-lock condition is reflected in $z_k^{(0)}$. We also remind that the radiation wake functions are with finite duration, i.e., $\mathcal{W}_{\parallel}(z<0)=0, \mathcal{W}_{\parallel}(z>N_w\lambda_r)=0$.

Now we are ready to formulate the macroparticle equations of motion for the longitudinal dynamics in an SSMB storage ring. Inside the undulator, we denote the period-by-period mapping of the longitudinal phase space coordinate from the undulator entrance $(z_m^{(0)},\delta_m^{(0)})$ to the exit $(z_m^{(N_w)},\delta_m^{(N_w)})$, with the subscripts m being the revolution index and the superscript indicating the location of the undulator in terms of the undulator period. The superscript (0) refers to the undulator entrance and (N_w) corresponds to the undulator exit. On the mth turn, the equation of motion for the longitudinal displacement at the $(n+1)$th undulator period can be expressed as [45]

$$z_m^{(n+1)}=z_m^{(n)}-\eta_w\lambda_w\delta_m^{(n+1)}, \tag{31}$$

with the undulator slippage factor $\eta_w=-(1+\frac{K^2}{2})/\gamma_0^2$. The relative energy deviation $\delta=(\gamma-\gamma_0)/\gamma_0$ can be perturbed by the radiation wake

$$\delta_m^{(n+1)}=\delta_m^{(n)}+\frac{k_{s0}^2\lambda_w}{\eta_w}z_m^{(n)} -\sum_{k=0}^{m-1}\mathcal{W}_{\parallel}[(N_w-n)\lambda_r+z_m^{(n)}-z_k^{(0)}], \tag{32}$$

where the scaled wake function is similarly defined as $\mathcal{W}_{\parallel}\equiv\frac{4\pi\varepsilon_0 N r_e\lambda_w}{\gamma_0}W_{\parallel}$. Here k_{s0} is characteristic of the longitudinal focusing provided by the external laser in the cavity modulator [44,45]. When the electron bunch leaves the undulator, let us define $(z_{m,\mathrm{fin}},\delta_{m,\mathrm{fin}})=(z_m^{(N_w)},\delta_m^{(N_w)})$. The phase space mapping from the undulator exit to the entrance of the next turn $(z_{m,\mathrm{fin}},\delta_{m,\mathrm{fin}})\to(z_{m+1,\mathrm{ini}},\delta_{m+1,\mathrm{ini}})=(z_{m+1}^{(0)},\delta_{m+1}^{(0)})$ can be formulated using the linear matrix

$$\begin{bmatrix}z_{m+1,\mathrm{ini}}\\ \delta_{m+1,\mathrm{ini}}\end{bmatrix}=\begin{pmatrix}1 & -\eta_{\mathrm{ring}}(C_{\mathrm{tot}}-L_w)\\ 0 & 1\end{pmatrix}\begin{bmatrix}z_{m,\mathrm{fin}}\\ \delta_{m,\mathrm{fin}}\end{bmatrix}, \tag{33}$$

where η_{ring} refers to the storage ring phase slippage factor, the total circumference C_{tot} involves the modulator and the remaining storage ring, $C_{\mathrm{tot}}=L_w+C_{\mathrm{ring}}$.

To further simplify Eqs. (31)–(33) on the turn-by-turn basis, we define the undulator-averaged phase space coordinates as [45]

$$\bar{z}_m=\frac{1}{N_w}\sum_{n=1}^{N_w}z_m^{(n)},\qquad \bar{\delta}_m=\frac{1}{N_w}\sum_{n=1}^{N_w}\delta_m^{(n)}, \tag{34}$$

then Eqs. (31)–(33) can be combined into one set of difference equations

$$\frac{\mathrm{d}\bar{z}_m}{\mathrm{d}m}=-(\eta_w L_w+\eta_{\mathrm{ring}}C_{\mathrm{ring}})\bar{\delta}_m, \tag{35}$$

with $C_{\mathrm{ring}}=C_{\mathrm{tot}}-L_w$

$$\frac{\mathrm{d}\bar{\delta}_m}{\mathrm{d}m}=\frac{k_{s0}^2L_w}{\eta_w}\bar{z}_m-\mathbb{W}'\sum_{k=0}^{m-1}(\bar{z}_m-\bar{z}_k), \tag{36}$$

in which the longitudinal synchrotron oscillation tune for the entire ring $\nu_{s0,\mathrm{tot}}^2=\frac{k_{s0}^2L_w^2}{4\pi^2}\frac{\eta_wL_w+\eta_{\mathrm{ring}}C_{\mathrm{ring}}}{\eta_wL_w}$. The explicit expressions of $\mathbb{W}'$ with detailed derivations can be found in Appendix B. Here, we note that $\mathbb{W}'$ has no m-dependence after the sum over p; the information of the radiation fields generated by a turn-by-turn circulating electron was contained in $\bar{z}_k$. Equations (35) and (36) are coupled linear equations and can be cast into a matrix equation

$$\begin{aligned}\begin{bmatrix}\bar{z}_{m+1}\\ \bar{\delta}_{m+1}\end{bmatrix}&=\begin{pmatrix}1 & -\eta_{\mathrm{ring}}C_{\mathrm{ring}}\\ 0 & 1\end{pmatrix}\left\{\begin{pmatrix}1 & -\eta_wL_w\\ \frac{k_{s0}^2L_w}{\eta_w}-m\mathbb{W}' & 1\end{pmatrix}\begin{bmatrix}\bar{z}_m\\ \bar{\delta}_m\end{bmatrix}+\sum_{k=0}^{m-1}\begin{pmatrix}0 & 0\\ \mathbb{W}' & 0\end{pmatrix}\begin{bmatrix}\bar{z}_k\\ \bar{\delta}_k\end{bmatrix}\right\}\\ &\approx\begin{pmatrix}1 & -(\eta_wL_w+\eta_{\mathrm{ring}}C_{\mathrm{ring}})\\ \frac{k_{s0}^2L_w}{\eta_w}-m\mathbb{W}' & 1\end{pmatrix}\begin{bmatrix}\bar{z}_m\\ \bar{\delta}_m\end{bmatrix}+\begin{pmatrix}0 & 0\\ \mathbb{W}' & 0\end{pmatrix}\sum_{k=0}^{m-1}\begin{bmatrix}\bar{z}_k\\ \bar{\delta}_k\end{bmatrix}\end{aligned} \tag{37}$$

or in a more compact form

$$Y_{m+1} = \mathbf{A}_m Y_m + \mathbf{B}\sum_{k=0}^{m-1} Y_k. \tag{38}$$

The matrix $\mathbf{A}$ will not have time dependence if the potential well distortion effect is neglected. Similar to Sec. II A, we will solve Eq. (38) for the system (in)stability in the next subsection.

B. Obtaining secular equation

Similar to the Robinson instability case, we can perform the z-transform on Eq. (38) to obtain the secular equation. Using Eqs. (10) and (13), we have

$$\mathsf{z}\tilde{Y}(\mathsf{z}) - \mathsf{z}Y_0 = \mathbf{A}\tilde{Y}(\mathsf{z}) + \mathbf{B}\frac{\tilde{Y}(\mathsf{z})}{\mathsf{z}-1}, \tag{39}$$

where we have used

$$\mathcal{Z}\left[\sum_{k=0}^{m-1} Y_k\right] = \frac{\tilde{Y}(\mathsf{z})}{\mathsf{z}-1}. \tag{40}$$

Solving Eq. (39) for $\tilde{Y}$ gives

$$\tilde{Y}(\mathsf{z}) = \frac{\mathsf{z}}{\mathsf{z}\mathbb{I} - \mathbf{A} - \frac{\mathbf{B}}{\mathsf{z}-1}} Y_0. \tag{41}$$

The system stability is determined by $\det(\mathsf{z}\mathbb{I} - \mathbf{A} - \frac{\mathbf{B}}{\mathsf{z}-1}) = 0$. That is

$$\det\begin{pmatrix} \mathsf{z}-1 & \eta_w L_w + \eta_{\rm ring} C_{\rm ring} \\ -\frac{k_{s0}^2 L_w}{\eta_w} - \frac{\mathbb{W}'}{\mathsf{z}-1} & \mathsf{z}-1 \end{pmatrix} = 0 \tag{42}$$

or

$$(\mathsf{z}-1)^2 + (\eta_w L_w + \eta_{\rm ring} C_{\rm ring})\left(\frac{k_{s0}^2 L_w}{\eta_w} + \frac{\mathbb{W}'}{\mathsf{z}-1}\right) = 0. \tag{43}$$

Similarly, we let $\mathsf{z} = e^{i\Omega T_0}$, with Ω in general a complex quantity. Then Eq. (43) can be written as

$$\Omega^3 - \omega_{s0,\rm tot}^2 \Omega + i\hat{\mathbb{W}} = 0, \tag{44}$$

with $\omega_{s0,\rm tot}^2 = \frac{k_{s0}^2 L_w^2}{T_0^2}\frac{\eta_w L_w + \eta_{\rm ring} C_{\rm ring}}{\eta_w L_w}$ and $\hat{\mathbb{W}} = \frac{\mathbb{W}'}{T_0^3}(\eta_w L_w + \eta_{\rm ring} C_{\rm ring})$. Here the explicit expression of $\mathbb{W}'$ can be found in Eq. (B4). Note that $\hat{\mathbb{W}}$ is a real quantity. Here we remind that the longitudinal single-particle optics stability requires $\eta_w L_w + \eta_{\rm ring} C_{\rm ring} < 0$.

For the moment we have obtained the secular equation [Eq. (44)] for the coherent undulator radiation induced multiturn instability in a laser cavity modulator. Equation (44) can be solved analytically or numerically, given the $\omega_{s0,\rm tot}$ and $\hat{\mathbb{W}}$. The analytical expressions of the three roots can be involved [45]; we will not present them here. In the next subsection, we will demonstrate the above analysis with the turn-by-turn tracking simulations by taking a preliminary design example based on an SSMB storage ring.

C. Example: SSMB

In this section, we illustrate a preliminary SSMB design example as a practical application of the developed theoretical formulation. The SSMB storage ring aims to produce continuous wave, high average power, coherent radiations with the targeted radiation wavelength at 13.5 nm. The relevant beam and undulator parameters, for example, are largely based on Ref. [43] with slight modifications. To be specific, the reference electron energy is 400 MeV, the microbunch charge 6.4 fC ($\approx 0.4\times 10^5$ electrons), the undulator parameter $K = 4.2$, the corresponding undulator slippage factor about $-(1+K^2/2)/\gamma_0^2 \approx -1.6\times 10^{-5}$, the undulator period 2 cm, the total number of undulator periods $N_w = 100$, and the total storage ring circumference $C_{\rm tot} = 50$ m. For simplicity, we assume $\eta_{\rm ring} = 0$. Moreover, the laser modulator voltage $V_m = 0.51$ kV is much smaller than the targeted value of 0.51 MV. The corresponding $k_{s0} \approx 0.017 \approx 2\pi/367$ rad/m [45]. The smaller synchrotron oscillation in the undulator makes the theoretical prediction close and accurate to the turn-by-turn tracking simulations [see also Eq. (34)]. Both the numerical turn-by-turn tracking simulation and the theoretical predictions are shown in Fig. 3, where we have assumed the linearized wake function and neglected the potential well distortion effect. Figures 3(a) and 3(b)

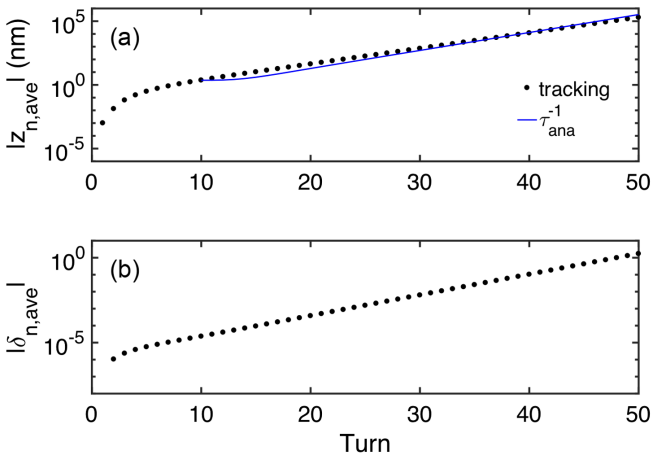

FIG. 3. Turn-by-turn evolution of the undulator-averaged phase space coordinates. In the tracking simulation, the radiation wake is linearized [Eq. (36)] and the laser modulator voltage $V_m = 0.51$ kV. The analytical prediction $\tau_{\rm ana}^{-1}$ is obtained by solving Eq. (44).

illustrate the undulator-averaged longitudinal phase space coordinates $\bar{z}_n$ and $\bar{\delta}_n$ for the first 50 turns. The macroparticle tracking simulations are performed by numerically iterating Eqs. (31) and (32) period by period inside the undulator and Eq. (33) turn by turn in the remaining storage ring. The theoretical prediction is also plotted in Fig. 3(a) as a comparison. Here we explain how the theoretical prediction (the blue curve) may be obtained. From Eq. (44), we first find the three instability growth rates $\mathrm{Im}\Omega$ ($\mathrm{Im}\Omega < 0$ for the exponential growth and $\mathrm{Im}\Omega > 0$ for the exponential damping). The asymptotic behavior of the longitudinal displacement $\bar{z}_n$ can be approximately written as the sum of the three roots in the form $|\bar{z}_n| \propto \sum_{j=0}^{2} e^{-\tau_j^{-1} T_0} \approx \sum_{j=0}^{2} e^{-(\mathrm{Im}\Omega_{j,I})T_0}$. To better compare with the tracking simulations, an initial value on the 10th turn is used as the starting value of the theoretical prediction. When evaluating the radiation impedance [Eq. (B4)], both using the continuous integration and the discrete sum give consistent and comparable predictions, and show reasonable agreement to the tracking simulation results.

Here we refer the interested reader to Ref. [45] for further discussions regarding this newly explored instability. In this section, we have formulated the single-bunch multiturn instability in the laser cavity modulator of an SSMB storage ring. In the following section, we will discuss and compare such an instability with the Robinson instability introduced in Sec. II and later the FEL instability in Sec. V.

IV. DISCUSSION

We have introduced in the previous two sections the single-bunch multiturn instabilities driven by the long-range rf cavity wake in a conventional storage ring (Sec. II) and the coherent undulator radiation in the laser cavity modulator of an SSMB storage ring (Sec. III). In this section, we will compare and discuss the two instabilities on the respective wake functions and the underlying mechanisms. Figure 4 illustrates the wake functions a circulating bunch on the fourth turn ($k = 3$) may experience in the rf cavity [Fig. 4(a)] and in the laser cavity modulator [Fig. 4(b)]. The wake functions produced on the previous three turns $k = 0, 1, 2$ are marked as red, orange, and green, respectively. In Fig. 4(a), the wake functions exhibit a translational or shift pattern with the ring circumference (plus small correction due to synchrotron oscillation of the circulating bunch). The localized rf cavity wakes behave like the standing waves (the finite Q value leads to field decay) and the beam bunch samples the successive parts of the wakes on each turn. Typically the rf cavity is considered a lumped element with zero length and a vanishing phase slippage factor. The situation becomes different in Fig. 4(b). Now the finite-duration radiation wakes are not localized but propagate along the undulator, although confined in the cavity modulator. The phase-lock

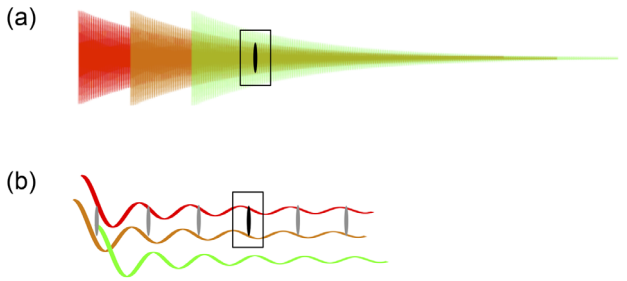

FIG. 4. Illustration of (a) the conventional long-range wake functions generated in an RF cavity; (b) the radiation wake functions produced by the circulating electrons in a laser cavity modulator. In (a) the wake function is localized and the negative longitudinal bunch coordinate z is to the right, referring to the bunch tail. In (b) the radiation wake is propagating to the right with the positive longitudinal bunch coordinate z. A small black box enclosing an electron bunch indicates a relative position, at which the passing bunch receives the energy kick from the wake functions. The gray microbunches in (b) correspond to different locations in the undulator due to the radiation slippage effect. See context for more explanation.

condition, as a result of the effective interaction between the external laser and the circulating bunch, assures that the bunch always meets the same phase space bucket at the undulator entrance. On each turn at the undulator entrance, the beam bunch can only sample the radiation wakes within the bucket width. See the rightmost gray microbunch in Fig. 4(b). When the bunch traverses along the undulator, the radiation field slips ahead for λ_r per undulator period. Then the beam bunch receives the varying parts of the wakes period by period from the undulator entrance to the exit. The small black box enclosing an electron bunch in Fig. 4(b) illustrates the bunch at the third undulator period. Here we note that Figs. 4(a) and 4(b) represent distinct physical length scales, though the two plots are drawn on a visually comparable scale.

The distinctive features of the respective wake functions lead to the different summation forms of the wake functions in the macroparticle equations of motion in the time domain [see Eqs. (9) and (38)]. When transforming to the frequency domain, such a distinction results in different secular equations. For the case of Robinson instability, it is the convolution-type sum Eq. (9) that leads to the quadratic secular equation [Eq. (16)]. The two roots represent the exponential growth and damping rate. For the case of the coherent undulator radiation induced multiturn instability, the wake sum of nonconvolution type Eq. (38) makes the cubic equation [Eq. (43)]. The three solutions, after a proper transformation, would represent exponential growth, exponential damping, and purely sinusoidal oscillation. Moreover, it is the real part of the impedance that contributes to the instability growth rate for the Robinson case [see Eq. (20)], while for our case, the instability growth is determined by the imaginary part of the impedance [see Eqs. (44) and (B4)]. Here we provide another

TABLE I. Comparison of the rf cavity wake induced Robinson instability and the single-bunch multiturn (SBMT) instability in the laser cavity modulator.

	Robinson	SBMT
Mechanism	Long-range wake in an rf cavity	Short-range radiation wake in a cavity modulator
Wake sum (Time domain)	$\sum_{k=0}^{n-1} W'_{\parallel}(nC-kC)z_k$	$(\sum_{p=0}^{N_w-1} W'_{\parallel}[(N_w-p)\lambda_r])(\sum_{k=0}^{m-1}\bar{z}_k)$
Impedance term (frequency domain)	$\tilde{W}'_{\parallel}(\mathsf{z})\tilde{Y}(\mathsf{z})$	$\frac{\mathbb{W}'}{\mathsf{z}-1}\tilde{Y}(\mathsf{z})$
Growth rate	$\tau^{-1}\propto\sum(p\omega_0+\omega_s)\mathrm{Re}Z_{\parallel}(p\omega_0+\omega_s)$	$\tau^{-1}\propto\sum(\eta_w L_w+\eta_{\mathrm{ring}}C_{\mathrm{ring}})n\mathrm{Im}Z_{\parallel}(n)$
Type	Absolute	Convective

aspect to draw an analogy between the two instabilities from plasma physics [51]. As the rf cavity wakes are localized, the Robinson instability can be considered as a type of absolute instability, where the unstable motion grows in time (turn after turn). In contrast, the coherent radiation wakes propagate inside the cavity modulator, and the unstable motion of the circulating bunch may exhibit growth both in time (turn after turn) and in space, i.e., travelling along the region of the perturbing source of finite duration inside the undulator. This belongs to the convective instability in plasma physics.

Before ending this section, we summarize the comparison of the two instability mechanisms in Table I. In the next section, we shall consider a special case of the multiturn instability in the laser cavity modulator in order to relate to the FEL instability.

V. FEL INSTABILITY

In formulating the multiturn instability in a laser cavity modulator, we have obtained the cubic dispersion or secular equation. Since the dispersion relation of the FEL instability is also a cubic equation [50,52], we might be tempted to relate the multiturn instability to the FEL instability in some special situation.

A. A special case of multiturn instability

When an electron bunch circulates in an SSMB storage ring, it would not suffer the radiation fields generated in the laser cavity modulator until the electron bunch would complete one revolution and come back to the undulator. If we try to draw an analogy between the multiturn situation and the FEL process, we may treat the electron bunch that would arrive after completing one revolution as the *test* bunch. The test bunch will experience the radiation wakes generated by the *source* bunches. Notice that it is still a single bunch that plays the two roles. Moreover, we require that the undulator to be a single-period undulator, i.e., $N_w=1, L_w=\lambda_w$. The storage ring also must not introduce any additional longitudinal slippage, i.e., $\eta_{\mathrm{ring}}=0$. Based on the aforementioned special case, we have the macroparticle equations of motion [see also Eqs. (35) and (36)]

$$\frac{\mathrm{d}z_m}{\mathrm{d}m}=-\eta_w\lambda_w\delta_m \tag{45}$$

and

$$\frac{\mathrm{d}\delta_m}{\mathrm{d}m}=\frac{k_{s0}^2\lambda_w}{\eta_w}z_m-\mathcal{W}'_{\parallel}(\Delta L)\sum_{k=0}^{m-1}(z_m-z_k). \tag{46}$$

Here the bar has been removed because of the single-period undulator. Similarly, the radiation wake does not participate to the sum over the revolution turns. Here $\Delta L\approx\lambda_r$. The two coupled difference equations can be combined into one second-order difference equation, neglecting the parasitic loss

$$\frac{\mathrm{d}^2z_m}{\mathrm{d}m^2}+k_s^2\lambda_w^2z_m\approx-\eta_w\lambda_w\mathcal{W}'_{\parallel}(\Delta L)\sum_{k=0}^{m-1}z_k, \tag{47}$$

where the potential well distortion effect can be absorbed by redefining the synchrotron oscillation wavenumber

$$k_s^2=k_{s0}^2-\frac{\eta_w}{\lambda_w}\mathcal{W}'_{\parallel}(\Delta L)\sum_{k=0}^{m-1}z_k. \tag{48}$$

In what follows, we will drop the potential well distortion term for simplicity. Now we solve Eq. (47) for the corresponding secular equation. In Eq. (47), the second-order term can be written as the central difference form

$$z_{m+2}-2z_{m+1}+(k_{s0}^2\lambda_w^2+1)z_m=-\eta_w\lambda_w\mathcal{W}'_{\parallel}(\Delta L)\sum_{k=0}^{m-1}z_k. \tag{49}$$

Taking the z-transform on both sides and using the shifting property [Eq. (13)], we have

$$[\mathsf{z}^2\tilde{z}(\mathsf{z})-(z_0\mathsf{z}^2+z_1\mathsf{z})]-2[\mathsf{z}\tilde{z}(\mathsf{z})-z_0\mathsf{z}]+(k_{s0}^2\lambda_w^2+1)\tilde{z}(\mathsf{z})=-\eta_w\lambda_w\mathcal{W}'_{\parallel}(\Delta L)\frac{\tilde{z}(\mathsf{z})}{\mathsf{z}-1}, \tag{50}$$

with $z_{0,1}$ the initial conditions. The initial conditions are not of our interest; we only care about the system (in)stability.

Solving Eq. (50) for $\tilde{z}$, we obtain

$$\tilde{z}(\mathsf{z}) = \frac{\mathsf{z}[z_0\mathsf{z} + z_1 - 2z_0]}{(\mathsf{z}-1)^2 + k_{s0}^2\lambda_w^2 + \frac{\eta_w\lambda_w\mathcal{W}_\parallel'(\Delta L)}{\mathsf{z}-1}}. \tag{51}$$

Again, the system stability is determined by requiring that the determinant of the denominator be zero, i.e.,

$$(\mathsf{z}-1)^2 + k_{s0}^2\lambda_w^2 + \frac{\eta_w\lambda_w\mathcal{W}_\parallel'(\Delta L)}{\mathsf{z}-1} = 0. \tag{52}$$

Now we let $\mathsf{z} = e^{i\Omega T_0}$ with $|\Omega T_0| \ll 1$, thus

$$\Omega^3 - \omega_{s0}^2\Omega + i\frac{c\eta_w\mathcal{W}_\parallel'(\Delta L)}{\lambda_w^2} = 0. \tag{53}$$

To further simplify the expression, we introduce the shorthand notations

$$A = -\frac{c\eta_w\mathcal{W}_\parallel'(\Delta L)}{\lambda_w^2} > 0 \quad \text{and} \quad \mu = i\frac{\Omega}{A^{1/3}}, \tag{54}$$

with A being a real quantity and μ, in general, a complex quantity. When $\omega_{s0} \to 0$, Eq. (53) can be simplified as

$$\mu^3 = 1, \tag{55}$$

which gives the solutions $\mu = 1, \frac{-1+\sqrt{3}i}{2}, \frac{-1-\sqrt{3}i}{2}$. These three roots lie on the unit circle with $|\mu| = 1$. Due to the slightly different notations adopted in our analysis, the most unstable root refers to $\mu = 1$, which corresponds to the instability growth rate $\Omega = -iA^{1/3}$. A more explicit expression of the dominant instability growth rate can be written as

$$\tau^{-1} = \mathrm{Im}\Omega = -A^{1/3} = -\left[-\frac{c\eta_w\mathcal{W}_\parallel'(\Delta L)}{\lambda_w^2}\right]^{\frac{1}{3}}. \tag{56}$$

B. Using collective variables

The most elegant description that captures the essence of the 1D high-gain FEL model can be based on the collective variable approach [50,52]. Here we will not derive but only quote the three dynamical equations

$$\begin{aligned}\frac{d\mathcal{A}}{d\hat{s}} &= -\mathcal{B}\\ \frac{d\mathcal{B}}{d\hat{s}} &= -i\mathcal{P}\\ \frac{d\mathcal{P}}{d\hat{s}} &= \mathcal{A},\end{aligned} \tag{57}$$

where $\mathcal{A}$ is the scaled complex electric field, $\mathcal{P}$ is the energy modulation, and $\mathcal{B}$ is the bunching factor, which reflects the microbunching due to the longitudinal slippage in the undulator. In Eq. (57), the scaled dimensionless path length $\hat{s}$ is defined as $\hat{s} = 2k_w\rho s$, with the Pierce parameter [50,52]

$$\hat{s} = 2k_w\rho s, \rho = \left[\frac{1}{8\pi}\frac{I_b}{I_A}\left(\frac{K[JJ]}{1+\frac{K^2}{2}}\right)^2\frac{\gamma\lambda_r^2}{2\pi\sigma_\perp^2}\right]^{\frac{1}{3}}, \tag{58}$$

where

$$[JJ] = J_0(\chi) - J_1(\chi), \tag{59}$$

with $\chi = \frac{K^2}{4+2K^2}$.

The three first-order differential equations can be combined as a third-order differential equation

$$\frac{d^3\mathcal{A}}{d\hat{s}^3} = i\mathcal{A}. \tag{60}$$

The dispersion or secular relation can be obtained by letting $\mathcal{A}(\hat{s}) \propto e^{-i\kappa\hat{s}}$, with κ being a complex quantity [50]. Substituting into Eq. (60) leads to

$$\kappa^3 = 1. \tag{61}$$

Although Eq. (61) has the same form as Eq. (55), the most unstable root corresponds to $\kappa = \frac{-1+\sqrt{3}i}{2}$. This does not affect the physical essence. The long-term behavior can be obtained by substituting the imaginary part of κ to $e^{-i\kappa\hat{s}}$.

C. Example

Let us now demonstrate the analyses in Sec. V A and Sec. V B by a numerical, artificial example. Assume the electron reference energy is 400 MeV, the bunch charge 10 fC ($\approx 0.625 \times 10^5$ electrons), the undulator parameter $K = 4.2$, the undulator slippage factor still -1.6×10^{-5}, the undulator period 2 cm, and $\eta_{\mathrm{ring}} = 0$. When considering the dynamical system as a single-pass system (Sec. V B), the number of undulator periods is set $N_w = 100$. When treating the system as the modified single-bunch multiturn (SBMT) case (Sec. V A), we require $N_w = 1, L_w = \lambda_w$, and the number of revolutions $m = 100$. Based on the numerical setup, Fig. 5 shows the longitudinal displacement as a function of s by comparing the results from the modified SBMT model and the 1D FEL high-gain model. The black solid line, based on the modified single-bunch multiturn formulation (Sec. V A), is obtained by iterating Eqs. (45) and (46) turn after turn and exhibits an exponentially growing behavior at a larger $\hat{s}$. The blue dotted line is evaluated by solving the secular equation [Eq. (56)] for the instability growth rate, also based on Sec. V A. The theoretical prediction of the red dashed line is based on

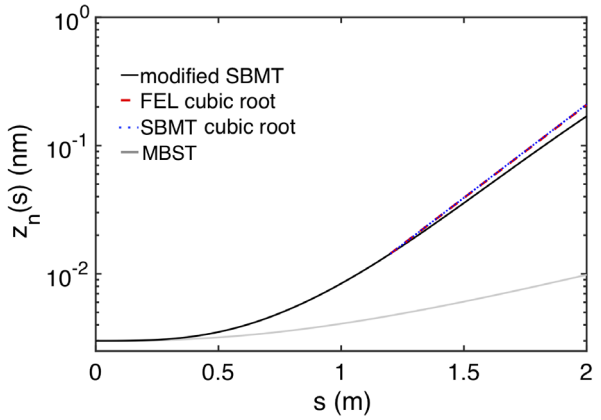

FIG. 5. Longitudinal displacement as a function of s. The black solid line is obtained by the modified single-bunch multiturn (SBMT) model; the red dashed line obtained by the FEL cubic equation [Eq. (60)]; the blue dotted line from the cubic root of the modified SBMT [Eq. (56)]. The gray solid line refers to the multibunch single-turn (MBST) case. In the calculations, we assume $N = 0.625 \times 10^5$ (10 fC), $V_m = 0$, $H_{\max} = 1$, and the initial conditions are set $z_0 = 3 \times 10^{-3}$ nm and $\delta_0 = 0$. Here the analytical predictions are fitted at $s = 1.2$ m.

the collective variable approach in the 1D high-gain FEL model, very close to that predicted by the modified SBMT model. When using the collective variable approach, we further assume $\sigma_\perp \approx 5\ \mu$m, $\sigma_z \approx \lambda_r$, $I_b \approx Nec/2.35\sigma_z \approx 800$A, thus the corresponding Pierce parameter $\rho \approx 0.0285$. Here we remind that this example is somewhat artificial; some of the parameters may not be practical. For example, the Pierce parameter is about 1 order of magnitude larger than the typical one ($\approx 10^{-3}$), resulting in a much reduced FEL gain length. However, it may have been sufficient to demonstrate the physical essence emphasized here.

In addition to the modified SBMT model, belonging to the single-bunch multiturn case, i.e., $N_w = 1, m = 100$, we further illustrate another similar situation based on the coherent undulator radiation induced multibunch single-turn (MBST) BBU model [44]. Here we shall consider $N_w = 100$, $N_b = 100$, with N_b being the number of microbunches. In Ref. [44], we have the macroparticle equations of motion for the nth microbunch with the bunch spacing equal to the resonant radiation wavelength

$$\frac{\mathrm{d}^2 z_n}{\mathrm{d}s^2} + k_{s0}^2 z_n \approx \frac{4\pi\epsilon_0 N r_e \eta_w}{\gamma} \sum_{j=0}^{N_b-1} (z_n - z_j) W_\parallel'[(n-j)\lambda_r] \Theta(p+j-n), \tag{62}$$

where p is defined such that $p\lambda_w < s < (p+1)\lambda_w$, and Θ is the Heaviside step function, reflecting the radiation slippage effect in the single-pass beam transport. The function Θ assures that the radiation wake in Eq. (62) can only take a value when the radiation field generated from the trailing microbunch takes over the test bunch.

The gray solid line in Fig. 5, based on the numerical results of Eq. (62), shows the longitudinal displacement of the most leading microbunch. We note that the instability growth rate of the most leading microbunch by such longitudinal multibunch BBU is slower than those of the modified SBMT and the FEL models. This is because the intervals between the trailing microbunches and the test bunch (the most leading one) are no longer λ_r for all microbunches but $(n-j)\lambda_r$. The radiation wakes from those farther microbunches have a relatively minor effect on the test bunch. For the modified SBMT model, in contrast, the driving sources always come from the following source bunches with $\Delta L \approx \lambda_r$. This can be traced back to the phase-lock condition. For the FEL case, the phase-lock condition is reduced to the undulator resonance condition. It is indeed such an internal phase lock that leads to the high-gain FEL instability. While the radiation field slips over the electron bunch, it coherently interacts with the electron beam, e.g., continuously extracting the energy from the electrons, when the system satisfies the resonance condition.

VI. SUMMARY

In this paper, we have outlined the theoretical formulation of the Robinson instability, a single-bunch multiturn instability driven by the rf cavity wake. We then introduced a recently explored multiturn collective effect driven by coherent undulator radiation in the laser cavity modulator of an SSMB storage ring. In both cases, the macroparticle equations of motion are solved by the z-transform to obtain the secular equation. A closer examination of the respective physical mechanisms reveals that the different forms of the secular equations can be traced back to the sum of the wake functions. The summation of convolution type leads to the quadratic secular equation, while that of nonconvolution type may result in the cubic equation, as the recently explored multiturn instability. Table I summarizes the key differences between the two types of instabilities.

The obtained cubic dispersion equation can be related to the FEL instability as a special case of the single-period undulator with vanishing storage ring slippage factor, $N_w = 1$ and $\eta_{\mathrm{ring}} = 0$. Using a numerical example, this special case is compared with a 1D high-gain FEL model based on the collective variable approach and is found that the reduced secular equation can capture the 1D FEL essence. The phase-lock condition plays an essential role in the multiturn instability and, when reduced to a special case this condition is connected to the resonance condition on the FEL process. Throughout the comparative studies, we shall gain a deeper understanding of this newly explored instability mechanism.

All the above discussions are made from a view of the theoretical formulation. From a practical aspect, a more

detailed, in-depth study on the coherent radiation induced single-bunch multiturn instability in the laser cavity modulator has been recently submitted [45], with an extension of the analysis on the multibunch multiturn collective dynamics is ongoing.

ACKNOWLEDGMENTS

The author wishes to show his appreciation to Prof. A. W. Chao for his insightful comments and encouragement. He also acknowledges Mr. Kumamoto for his help with the preparation of this manuscript. This work is supported by the Fundamental Research Funds for the Central Universities under Project No. 5003131049 and the National Natural Science Foundation of China under Project No. 11905073.

APPENDIX A: DERIVATION OF $\tilde{\mathcal{W}}'_{\parallel}$ IN EQ. (15)

This appendix is to evaluate $\tilde{\mathcal{W}}'_{\parallel}$ in Eqs. (15)–(17). According to the definition of the z-transform and $\mathsf{z} = e^{i\Omega T_0}$, we have

$$\begin{aligned}\tilde{\mathcal{W}}'_{\parallel}(\mathsf{z}) &= \frac{4\pi\epsilon_0 N r_e}{\gamma_0}\mathcal{Z}[W'_{\parallel}(z)] \\ &= \frac{4\pi\epsilon_0 N r_e}{\gamma_0}\sum_{j=0}^{\infty} W'_{\parallel}(-jC)\mathsf{z}^{-j} \\ &= \frac{4\pi\epsilon_0 N r_e}{\gamma_0}\frac{i}{2\pi c}\sum_{j=0}^{\infty}\int_{-\infty}^{\infty}\omega Z_{\parallel}(\omega)e^{-ij\omega T_0}e^{+ij\Omega T_0}\mathrm{d}\omega \\ &= \frac{4\pi\epsilon_0 N r_e}{\gamma_0}\frac{i\omega_0}{2\pi c}\int_{-\infty}^{\infty}\omega Z_{\parallel}(\omega)\left[\sum_{j=0}^{\infty}e^{-ij\omega T_0}e^{+ij\Omega T_0}\right] \\ &\quad\times \mathrm{d}\frac{\omega}{\omega_0}, \end{aligned} \tag{A1}$$

where the sum in the square bracket of the last equality can be easily obtained

$$\sum_{j=0}^{\infty}e^{-ij\omega T_0}e^{+ij\Omega T_0} = \frac{e^{-i(\omega-\Omega)T_0}}{e^{-i(\omega-\Omega)T_0}-1}. \tag{A2}$$

Because Eq. (A2) as a function of ω behaves like a δ-function train, we may further simplify Eq. (A1)

$$\begin{aligned}\tilde{\mathcal{W}}'_{\parallel}(\mathsf{z}) &= \frac{4\pi\epsilon_0 N r_e}{\gamma_0}\frac{i\omega_0}{2\pi c}\int_{-\infty}^{\infty}\omega Z_{\parallel}(\omega)\left[\frac{e^{-i(\omega-\Omega)T_0}}{e^{-i(\omega-\Omega)T_0}-1}\right]\mathrm{d}\frac{\omega}{\omega_0} \\ &\approx \frac{4\pi\epsilon_0 N r_e}{\gamma_0}\frac{i\omega_0}{2\pi c}\int_{-\infty}^{\infty}\omega Z_{\parallel}(\omega)\left[\sum_{p=-\infty}^{\infty}\delta(\omega-\Omega-p\omega_0)\right] \\ &\quad\times \mathrm{d}\frac{\omega}{\omega_0} \\ &= \frac{4\pi\epsilon_0 N r_e}{\gamma_0}\frac{i}{cT_0}\sum_{p=-\infty}^{\infty}(\Omega+p\omega_0)Z_{\parallel}(\Omega+p\omega_0). \end{aligned} \tag{A3}$$

After substituting Eq. (A3) in Eq. (17), we obtain Eq. (18).

APPENDIX B: DERIVATION OF $\mathbb{W}'$ IN EQ. (36)

Here we complete the derivation of Eq. (36) by determining the explicit expression of $\mathbb{W}'$. First, we linearize Eq. (30) by assuming $(N_w - p)\lambda_r \gg (z_m^{(p)} z_n^{(0)})$

$$\begin{aligned}&\sum_{p=0}^{N_w-1}\mathcal{W}_{\parallel}[(N_w-p)\lambda_r + z_m^{(p)} - z_k^{(0)}] \\ &\approx \sum_{p=0}^{N_w-1}\{\mathcal{W}_{\parallel}[(N_w-p)\lambda_r] + (z_m^{(p)} - z_k^{(0)})\mathcal{W}'_{\parallel}[(N_w-p)\lambda_r]\}. \end{aligned} \tag{B1}$$

The first term on the right-hand side corresponds to the parasitic loss of the entire bunch. The second term proportional to $z_m^{(p)}$ can be related to the effect of the potential well distortion. The last term proportional to $z_k^{(0)}$, of our most interest, participates in the collective dynamics. Note that the $z_k^{(0)}$ reflects the concept of the phase lock between the circulating electron bunch and the external laser. Now $\mathbb{W}'$ involves the sum of $\mathcal{W}'_{\parallel}$ over the undulator period p. According to the definition of the wake function in terms of the impedance, we have

$$\begin{aligned}\mathbb{W}' &= \sum_{p=0}^{N_w-1}\mathcal{W}'_{\parallel}[(N_w-p)\lambda_r] \\ &= \frac{4\pi\epsilon_0 N r_e\lambda_w}{\gamma_0}\sum_{p=0}^{N_w-1}W'_{\parallel}[(N_w-p)\lambda_r] \\ &= \frac{4\pi\epsilon_0 N r_e\lambda_w}{\gamma_0}\frac{i}{2\pi c}\int_{-\infty}^{\infty}\omega Z_{\parallel}(\omega)\left[\sum_{p=0}^{N_w-1}e^{i\frac{\omega}{c}(N_w-p)\lambda_r}\right]\mathrm{d}\omega, \end{aligned} \tag{B2}$$

in which the sum in the square bracket of the last equality can be expressed as

$$\sum_{p=0}^{N_w-1}e^{i\frac{\omega}{c}(N_w-p)\lambda_r} = e^{i\frac{\omega}{c}(\frac{N_w+1}{2})\lambda_r}\frac{\sin\frac{N_w}{2}\frac{\omega}{c}\lambda_r}{\sin\frac{1}{2}\frac{\omega}{c}\lambda_r} = e^{i2\pi\tilde{k}(\frac{N_w+1}{2})}\frac{\sin N_w\pi\tilde{k}}{\sin\pi\tilde{k}}, \tag{B3}$$

where we have introduced the normalized wavenumber $\tilde{k} = k/k_r$. When $N_w \gg 1$, the ratio of sine functions in Eq. (B3) behaves like a δ-function train. Based on this observation, Eq. (B3) can be further simplified as

$$\mathbb{W}' = \frac{4\pi\epsilon_0 N r_e \lambda_w}{\gamma_0} \frac{ik_r^2 c N_w}{2\pi} \int_{-\infty}^{\infty} \tilde{k} Z_{\parallel}(\tilde{k}) \times \left[e^{i2\pi\tilde{k}\left(\frac{N_w+1}{2}\right)} \frac{\sin N_w \pi\tilde{k}}{N_w \sin \pi\tilde{k}} \right] \mathrm{d}\tilde{k} \approx \frac{4\pi\epsilon_0 N r_e \lambda_w}{\gamma_0} \frac{ik_r^2 c N_w}{2\pi} \sum_{n=-\infty}^{\infty} (-1)^{N_w n} n Z_{\parallel}(n), \quad \text{(B4)}$$

in which use of $\int(\ldots)\mathrm{d}\tilde{k} = \sum_{n=-\infty}^{\infty}(\ldots)\delta(\tilde{k}-n)$ has been made to convert the continuous integration to the discrete sum. We will use Eq. (B4) to evaluate $\mathbb{W}'$ in Eq. (36).

[1] Alexander Wu Chao, *Physics of Collective Beam Instabilities in High Energy Accelerators* (John Wiley & Sons, New York, 1993).

[2] King-Yuen Ng, *Physics of Intensity Dependent Beam Instabilities* (World Scientific, Singapore, 2006).

[3] W. K. H. Panofsky and R. B. Neal, Electrons accelerated to the 10-to 20-GeV range, Science **152**, 1353 (1966).

[4] W. K. H. Panofsky and M. Bander, Asymptotic theory of beam break-up in linear accelerators, Rev. Sci. Instrum. **39**, 206 (1968).

[5] Alexander W. Chao, Burton Richter, and Chi-Yuan Yao, Beam emittance growth caused by transverse deflecting fields in a linear accelerator, Nucl. Instrum. Methods **178**, 1 (1980).

[6] R. D. Kohaupt, Simplified presentation of head tail turbulence, DESY Report No. M-80/19, 1980, https://bib-pubdb1.desy.de/record/274891/files/Simplified.pdf.

[7] Richard Talman, The influence of finite synchrotron oscillation frequency on the transverse head-tail effect, Nucl. Instrum. Methods Phys. Res. **193**, 423 (1982).

[8] E. L. Saldin, E. A. Schneidmiller, and M. V. Yurkov, Klystron instability of a relativistic electron beam in a bunch compressor, Nucl. Instrum. Methods Phys. Res., Sect. A **490**, 1 (2002).

[9] S. Heifets, G. Stupakov, and S. Krinsky, Coherent synchrotron radiation instability in a bunch compressor, Phys. Rev. ST Accel. Beams **5**, 064401 (2002).

[10] Zhirong Huang and Kwang-Je Kim, Formulas for coherent synchrotron radiation microbunching in a bunch compressor chicane, Phys. Rev. ST Accel. Beams **5**, 074401 (2002).

[11] Marco Venturini, Microbunching instability in single-pass systems using a direct two-dimensional Vlasov solver, Phys. Rev. ST Accel. Beams **10**, 104401 (2007).

[12] Marco Venturini, Robert Warnock, and Alexander Zholents, Vlasov solver for longitudinal dynamics in beam delivery systems for x-ray free electron lasers, Phys. Rev. ST Accel. Beams **10**, 054403 (2007).

[13] Cheng-Ying Tsai and Weilun Qin, Semi-analytical analysis of high-brightness microbunched beam dynamics with collective and intrabeam scattering effects, Phys. Plasmas **28**, 013112 (2021).

[14] Marco Venturini, Robert Warnock, Ronald Ruth, and James A. Ellison, Coherent synchrotron radiation and bunch stability in a compact storage ring, Phys. Rev. ST Accel. Beams **8**, 014202 (2005).

[15] G. Stupakov and S. Heifets, Beam instability and microbunching due to coherent synchrotron radiation, Phys. Rev. ST Accel. Beams **5**, 054402 (2002).

[16] S. Heifets and G. Stupakov, Single-mode coherent synchrotron radiation instability, Phys. Rev. ST Accel. Beams **6**, 064401 (2003).

[17] S. Heifets, Single-mode coherent synchrotron radiation instability of a bunched beam, Phys. Rev. ST Accel. Beams **6**, 080701 (2003).

[18] Yunhai Cai, Linear theory of microwave instability in electron storage rings, Phys. Rev. ST Accel. Beams **14**, 061002 (2011).

[19] C.-Y. Tsai, D. Douglas, R. Li, and C. Tennant, Linear microbunching analysis for recirculation machines, Phys. Rev. Accel. Beams **19**, 114401 (2016).

[20] C.-Y. Tsai, Ya. S. Derbenev, D. Douglas, R. Li, and C. Tennant, Vlasov analysis of microbunching instability for magnetized beams, Phys. Rev. Accel. Beams **20**, 054401 (2017).

[21] K. A. Thompson and Ronald D. Ruth, Transverse and longitudinal coupled bunch instabilities in trains of closely spaced bunches, in *Proceedings of the 1989 IEEE Particle Accelerator Conference, Chicago, IL* (IEEE, New York, 1989), pp. 792–794.

[22] Karl L. F. Bane and Zenghai Li, Dipole mode detuning in the injector linacs of the NLC, Report No. SLAC-AP-134, 2000, https://accelconf.web.cern.ch/l00/papers/TUA06.pdf.

[23] D. Schulte, Multi-bunch calculations in the CLIC main linac, in *Proceedings of the 23rd Particle Accelerator Conference, Vancouver, Canada, 2009* (IEEE, Piscataway, NJ, 2009), pp. 4664–4666.

[24] Muhammad Shumail and Valery A. Dolgashev, Exact solution of multi-bunch instabilities for ultra-relativistic constant energy bunches in particle accelerators, Phys. Scr. **94**, 065208 (2019).

[25] Kenneth Wade Robinson, Stability of beam in radiofrequency system, Technical Report No. CEAL-1010, Cambridge Electron accelerator, MA, 1964, https://cds.cern.ch/record/905061/files/cer-002575271.pdf.

[26] Perry B. Wilson and James E. Griffin, High energy electron linacs; application to storage ring rf systems and linear colliders, AIP Conf. Proc. **87**, 450 (1982).

[27] Andrew M. Sessler and Vittorio G. Vaccaro, Longitudinal instabilities of azimuthally uniform beams in circular vacuum chambers with walls of arbitrary electrical properties, Technical Report No. CERN-67-02, 1967, https://cds.cern.ch/record/275815/files/CERN-67-02.pdf.

[28] A. G. Ruggiero and V. G. Vaccaro, The wake field of an oscillating particle in the presence of conducting plates with resistive terminations at both ends, Technical Report No. LNF-69/80, 1969.

[29] R. Bonifacio, F. Casagrande, G. Cerchioni, L. de Salvo Souza, P. Pierini, and N. Piovella, Physics of the high-gain FEL and superradiance, Riv. Nuovo Cimento (1978-1999) **13**, 1 (1990).

[30] Ya. S. Derbenev, J. Rossbach, E. L. Saldin, and V. D. Shiltsev, Microbunch radiative tail-head interaction,

Report Nos. PRINT-98-023, DESY-TESLA-FEL-95-05, 1995, https://inspirehep.net/literature/408530.

[31] J. B. Murphy, R. L. Gluckstern, and S. Krinsky, Longitudinal wake field for an electron moving on a circular orbit, Part. Accel. **57**, 9 (1996), https://cds.cern.ch/record/1120287/files/p9.pdf.

[32] E. L. Saldin, E. A. Schneidmiller, and M. V. Yurkov, On the coherent radiation of an electron bunch moving in an arc of a circle, Nucl. Instrum. Methods Phys. Res., Sect. A **398**, 373 (1997).

[33] Rui Li and Cheng-Ying Tsai, CSR impedance for non-ultrarelativistic beams, in *Proceedings of the 6th International Particle Accelerator Conference, IPAC-2015, Richmond, VA, 2015* (JACoW, Geneva, Switzerland, 2015), MOPMN004.

[34] Rui Li and Cheng-Ying Tsai, Entrance and exit CSR impedance for non-ultrarelativistic beam, in *Proceedings of the 8th International Particle Accelerator Conference, IPAC-2017, Copenhagen, Denmark, 2017* (JACoW, Geneva, Switzerland, 2017), WEPIK113.

[35] E. L. Saldin, E. A. Schneidmiller, and M. V. Yurkov, Radiative interaction of electrons in a bunch moving in an undulator, Nucl. Instrum. Methods Phys. Res., Sect. A **417**, 158 (1998).

[36] Juhao Wu, Tor O. Raubenheimer, and Gennady V. Stupakov, Calculation of the coherent synchrotron radiation impedance from a wiggler, Phys. Rev. ST Accel. Beams **6**, 040701 (2003).

[37] Alexander Wu Chao, Karl Hubert Mess *et al.*, *Handbook of Accelerator Physics and Engineering* (World scientific, Singapore, 2013).

[38] Daniel F. Ratner and Alexander W. Chao, Steady-State Microbunching in a Storage Ring for Generating Coherent Radiation, Phys. Rev. Lett. **105**, 154801 (2010).

[39] Yi Jiao, Daniel F. Ratner, and Alexander W. Chao, Terahertz coherent radiation from steady-state microbunching in storage rings with x-band radio-frequency system, Phys. Rev. ST Accel. Beams **14**, 110702 (2011).

[40] X. J. Deng, A. W. Chao, J. Feikes, W. H. Huang, M. Ries, and C. X. Tang, Single-particle dynamics of microbunching, Phys. Rev. Accel. Beams **23**, 044002 (2020).

[41] X. J. Deng, R. Klein, A. W. Chao, A. Hoehl, W. H. Huang, J. Li, J. Lubeck, Y. Petenev, M. Ries, I. Seiler *et al.*, Widening and distortion of the particle energy distribution by chromaticity in quasi-isochronous rings, Phys. Rev. Accel. Beams **23**, 044001 (2020).

[42] Xiujie Deng, Alexander Chao, Jörg Feikes, Arne Hoehl, Wenhui Huang, Roman Klein, Arnold Kruschinski, Ji Li, Aleksandr Matveenko, Yuriy Petenev *et al.*, Experimental demonstration of the mechanism of steady-state microbunching, Nature (London) **590**, 576 (2021).

[43] A. Chao, E. Granados, X. B. Huang, D. Ratner, and H.-W. Luo, High power radiation sources using the steady-state microbunching mechanism, in *Proceedings of the 7th International Particle Accelerator Conference, IPAC-2016, Busan, Korea, 2016* (JACoW, Geneva, Switzerland, 2016), TUXB01.

[44] C.-Y. Tsai, A. W. Chao, Y. Jiao, H.-W. Luo, M. Ying, and Q. Zhou, Coherent radiation induced longitudinal single-pass beam breakup instability of a steady-state microbunch train in an undulator, Phys. Rev. Accel. Beams **24**, 114401 (2021).

[45] C.-Y. Tsai *et al.*, Longitudinal single-bunch instabilities driven by coherent undulator radiation in the cavity modulator of a steady-state microbunching storage ring, arXiv:2205.15801.

[46] Sabor Elaydi, *An Introduction to Difference Equations* (Springer-Verlag, New York, 2005).

[47] Alexander Wu Chao, *Lectures on Accelerator Physics* (World Scientific, Singapore, 2020).

[48] Albert Hofmann, *The Physics of Synchrotron Radiation* (Cambridge University Press, Cambridge, England, 2004), Vol. 20.

[49] Helmut Wiedemann, *Particle Accelerator Physics*, 4th ed. (Springer Nature, 2015), https://link.springer.com/book/10.1007/978-3-319-18317-6.

[50] Kwang-Je Kim, Zhirong Huang, and Ryan Lindberg, *Synchrotron Radiation and Free-Electron Lasers* (Cambridge University Press, Cambridge, England, 2017).

[51] Richard J. Briggs, *Electron-stream Interaction with Plasmas* (MIT-Press, Cambridge, MA, 1964).

[52] R. Bonifacio, C. Pellegrini, and L. M. Narducci, Collective instabilities and high-gain regime free electron laser, AIP Conf. Proc. **118**, 236 (1984).